LETTER

Allosteric inhibition of SHP2 phosphatase inhibits cancers driven by receptor tyrosine kinases

Ying-Nan P. Chen[1], Matthew J. LaMarche[1], Ho Man Chan[1], Peter Fekkes[1], Jorge Garcia-Fortanet[1], Michael G. Acker[1], Brandon Antonakos[1], Christine Hiu-Tung Chen[1], Zhouliang Chen[1], Vesselina G. Cooke[1], Jason R. Dobson[1], Zhan Deng[1], Feng Fei[1], Brant Firestone[1], Michelle Fodor[1], Cary Fridrich[1], Hui Gao[1], Denise Grunenfelder[1], Huai-Xiang Hao[1], Jaison Jacob[1], Samuel Ho[1], Kathy Hsiao[1], Zhao B. Kang[1], Rajesh Karki[1], Mitsunori Kato[1], Jay Larrow[1], Laura R. La Bonte[1], Francois Lenoir[1], Gang Liu[1], Shumei Liu[1], Dyuti Majumdar[1], Matthew J. Meyer[1], Mark Palermo[1], Lawrence Perez[1], Minying Pu[1], Edmund Price[1], Christopher Quinn[1], Subarna Shakya[1], Michael D. Shultz[1], Joanna Slisz[1], Kavitha Venkatesan[1], Ping Wang[1], Markus Warmuth[1], Sarah Williams[1], Guizhi Yang[1], Jing Yuan[1], Ji-Hu Zhang[1], Ping Zhu[1], Timothy Ramsey[1], Nicholas J. Keen[1], William R. Sellers[1], Travis Stams[1] & Pascal D. Fortin[1]

The non-receptor protein tyrosine phosphatase SHP2, encoded by *PTPN11*, has an important role in signal transduction downstream of growth factor receptor signalling and was the first reported oncogenic tyrosine phosphatase[1]. Activating mutations of SHP2 have been associated with developmental pathologies such as Noonan syndrome and are found in multiple cancer types, including leukaemia, lung and breast cancer and neuroblastoma[1–5]. SHP2 is ubiquitously expressed and regulates cell survival and proliferation primarily through activation of the RAS–ERK signalling pathway[2,3]. It is also a key mediator of the programmed cell death 1 (PD-1) and B- and T-lymphocyte attenuator (BTLA) immune checkpoint pathways[6,7]. Reduction of SHP2 activity suppresses tumour cell growth and is a potential target of cancer therapy[8,9]. Here we report the discovery of a highly potent ($IC_{50} = 0.071\,\mu M$), selective and orally bioavailable small-molecule SHP2 inhibitor, SHP099, that stabilizes SHP2 in an auto-inhibited conformation. SHP099 concurrently binds to the interface of the N-terminal SH2, C-terminal SH2, and protein tyrosine phosphatase domains, thus inhibiting SHP2 activity through an allosteric mechanism. SHP099 suppresses RAS–ERK signalling to inhibit the proliferation of receptor-tyrosine-kinase-driven human cancer cells *in vitro* and is efficacious in mouse tumour xenograft models. Together, these data demonstrate that pharmacological inhibition of SHP2 is a valid therapeutic approach for the treatment of cancers.

To discover new cancer therapeutic targets, a deep-coverage, pooled short hairpin RNA (shRNA) library targeting 7,500 genes with 20 shRNAs per gene was screened across a panel of 250 cell lines from the Cancer Cell Line Encyclopedia (CCLE) (ref. 10 and Schlabach *et al.*, manuscript in preparation). An unbiased correlation analysis was performed and revealed that cell lines sensitive to SHP2 depletion are most sensitive to EGFR depletion ($P = 4.10 \times 10^{-8}$). When a subset of cell lines dependent on known receptor tyrosine kinases (RTKs) (such as EGFR, ERBB2, c-MET, and FLT3) and FRS2-dependent lines were considered as a class, a marked correlation emerged with sensitivity to SHP2 depletion (Fig. 1a and Extended Data Fig. 1, Fisher's exact $P < 4.45 \times 10^{-14}$). These findings provide a robust cross-validation of reports that RTK-driven cancer cells depend on SHP2 for survival[8,9]. Conversely, cell lines that were sensitive to KRAS, NRAS or BRAF depletion were refractory to SHP2 downregulation (Fig. 1b and Extended Data Fig. 1, Fisher's exact $P < 7.90 \times 10^{-5}$). To validate these findings further, doxycycline (dox)-inducible SHP2 shRNAs were introduced into cancer cells lines with distinct RTK alterations, including amplification of *EGFR* (MDA-MB-468, KYSE520), *ERBB2* (NCI-H2170), *FGFR2* (SUM52 and KATO III), and *EML4-ALK*

translocation (NCI-H2228). Consistent with the shRNA screening data, SHP2 depletion led to marked inhibition of colony formation in each of these RTK-dependent cancer cells (Extended Data Fig. 1a). Importantly, this was specific to RTK-dependent cell lines, as *BRAF*- and *KRAS*-mutated cells (A2058 and MDA-MB-231) showed no growth effect upon SHP2 depletion (Extended Data Fig. 1b). To evaluate the importance of SHP2 catalytic activity for the growth of sensitive cell lines, a complementation experiment was conducted by re-expressing shRNA-resistant alleles of wild-type SHP2 or the catalytically inactive SHP2[C459S] variant in MDA-MB-468 cells. SHP2 depletion inhibited the growth of MDA-MB-468 accompanied by reduced p-ERK levels (Fig. 1c, Extended Data Fig. 1a, c). Upon dox treatment, wild-type SHP2 and SHP2[C459S] were expressed at similar levels. Expression of wild-type SHP2, but not SHP2[C459S] restored p-ERK levels and cell growth (Fig. 1c, Extended Data Fig. 1c). Similar results were obtained with SUM52 cells (Extended Data Fig. 2). Therefore, SHP2 phosphatase activity is required for p-ERK activation and maintenance of cell growth in RTK-driven cancers.

On the basis of the shRNA screening results, we hypothesized that cells with constitutively activated RAS signalling would be insensitive to SHP2 inhibition. To test this hypothesis, SHP2-dependent SUM52 cells were transduced with a lentivirus carrying the *KRAS[G12V]* oncogene. Expression of KRAS[G12V] restored p-ERK levels and rendered these cells insensitive to SHP2 knockdown (Fig. 1d, Extended Data Fig. 1d). Furthermore, SHP2 depletion had no impact on cell growth and proliferation in MDA-MB-231 (KRAS[G13D]) or A2058 (BRAF[V600E]) cells (Extended Data Fig. 1b). These data strongly suggest that cancer cells carrying oncogenic *RAS/RAF* mutations will be refractory to SHP2 inhibition.

Efforts to discover small molecule therapeutics targeting protein tyrosine phosphatases (PTPs) have been challenged by the highly solvated and polar nature of the catalytic site, as exemplified by the SHP2 PTP domain[11–15]. To discover novel modes of phosphatase inhibition, we developed screening strategies aimed at identifying SHP2 allosteric inhibitors. SHP2 is activated by peptides and proteins containing appropriately spaced phospho-tyrosine residues that bind the N-terminal and C-terminal SH2 domains (denoted as N-SH2 and C-SH2, respectively) in a bidentate manner, releasing the auto-inhibitory interface and making the active site available for substrate recognition and turnover[16,17]. To discover inhibitors that could take advantage of this natural regulatory mechanism and lock SHP2 in an auto-inhibited conformation (Fig. 2a), a diverse library of 100,000 compounds were screened at $20\,\mu M$ against SHP2 (residues 1–525) that was partially activated using $0.5\,\mu M$ of a bisphosphorylated IRS-1
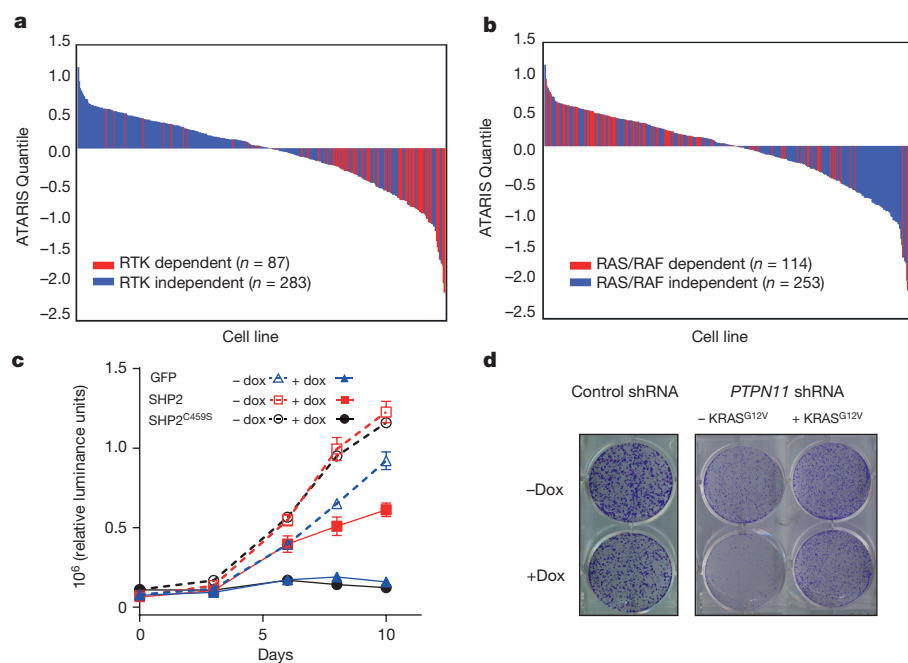
Figure 1 | Genetic validation of SHP2.
a, Waterfall plot showing the ATARIS Quantile score for SHP2 shRNAs coloured by the effect of RTK shRNA knockdown (ATARIS score < -1.0) in 370 cell lines. **b**, Waterfall plot showing the ATARIS Quantile score for SHP2 shRNAs coloured by the effect of shRNA knockdown of KRAS, NRAS or BRAF (ATARIS score < -1.0) in 367 cell lines. **c**, Cell proliferation in MDA-MB-468 SHP2 knockdown cells stably expressing GFP, wild-type haemagglutinin (HA)-tagged SHP2 or HA–SHP2^{C459S}. Cells were treated with dox (100 ng ml^{-1}) and cell growth was measured by CellTiter-Glo assay at the indicated times. Data presented as mean $\pm$ s.d. ($n = 3$). **d**, Colony formation of SHP2-depleted SUM52 cells stably expressing vector control or HA–KRAS^{G12V}. In **c** and **d**, dox treatment induces depletion of endogenous SHP2 protein and simultaneous expression of the exogenous proteins GFP, wild-type HA–SHP2, HA–SHP2^{C459S} or HA–KRAS^{G12V}.
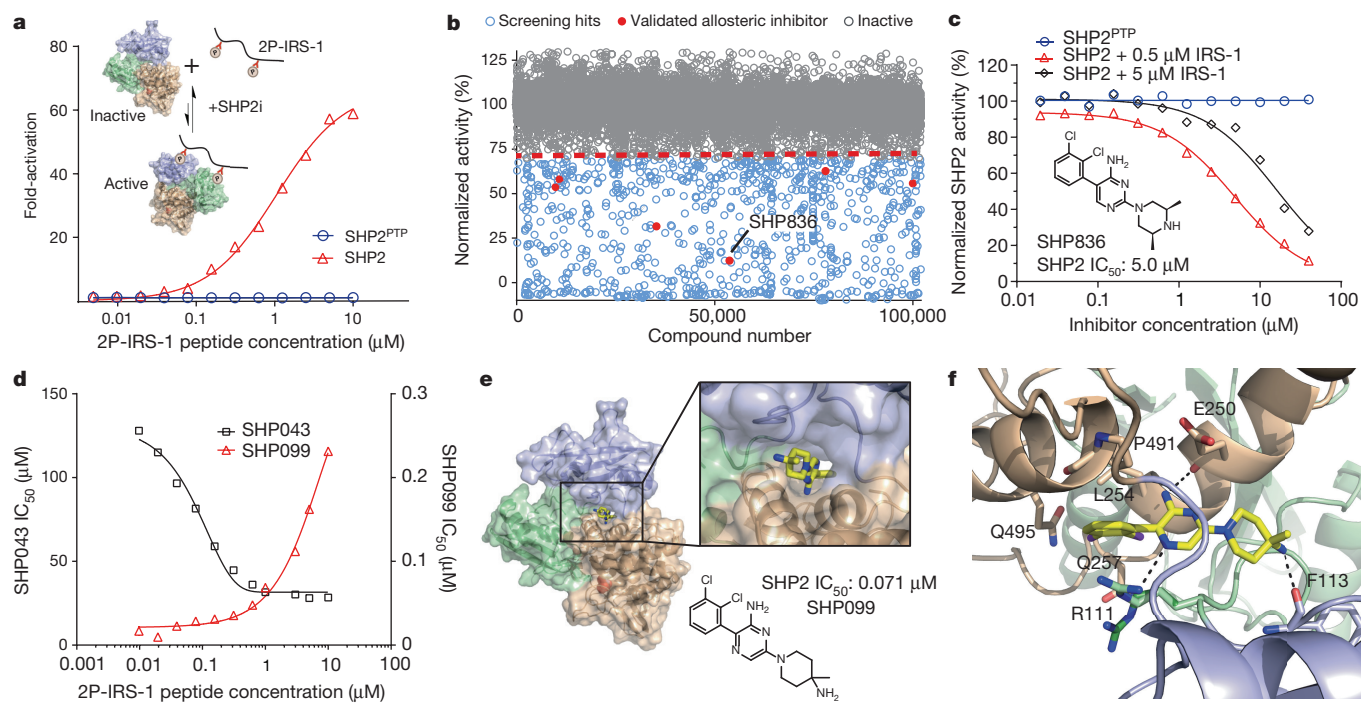

Figure 2 | Discovery of a SHP2 allosteric inhibitor. a, Schematic of SHP2 allosteric activation by 2P-IRS-1, highlighting an allosteric inhibitor that blocks the activation of SHP2 via the enrichment of its auto-inhibited conformer and dose-dependent activation of SHP2 by 2P-IRS-1 peptide. SHP2, SHP2^{PTP} and a dimethyl sulfoxide (DMSO) control were incubated with increasing concentrations of 2P-IRS-1 peptide. Biochemical activity was monitored using the DiFMUP (6,8-difluoro-4-methylumbelliferyl phosphate) substrate and normalized against the basal activity determined for each condition in the absence of 2P-IRS-1. SHP2i, SHP2 inhibitor. **b**, Primary screen was performed using a 100,000-molecule library. SHP2 was screened in the presence of 0.5 μM 2P-IRS-1 and 20 μM of each compound. The red dotted line represents the 30% inhibition threshold. The red circles represent the six validated allosteric inhibitors. SHP836 is labelled, and inhibited SHP activity by 87.6% The Z' factor determined for the screen was >0.9. **c**, Biochemical assay fingerprint observed with allosteric inhibitor SHP836. Inhibition of SHP2^{PTP} and SHP2 in the presence of 0.5 μM 2P-IRS-1 and 5 μM 2P-IRS-1. **d**, SHP2 inhibition by SHP099 and PTP active-site inhibitor SHP043 in the presence of various 2P-IRS-1 concentrations. **e**, Chemical structure of SHP099 and X-ray crystal structure of SHP2 in complex with SHP099 (PDB accession number 5EHR). Surface representation of SHP2 in complex with SHP099 bound in the central tunnel formed at the interface of the three domains (green, N-SH2; blue, C-SH2; tan, PTP domain). SHP2 is in the inactive conformation with the N-terminal SH2 domain fully occluding the entry of substrate to the active-site cysteine (shown in red). **f**, Key interactions between SHP099 and all three domains of SHP2 highlighted, including hydrogen bonds with Arg111 (N-SH2), Phe113 (C-SH2), and Glu250 (PTP). Data points along the line in **a**, **c** and **d** represent the mean of two replicate values.

peptide (2P-IRS-1). Nine hundred compounds were found to inhibit the enzyme by 30% or more (Fig. 2b) and further profiled in three distinct biochemical assays: (1) using a truncated form of SHP2 with the PTP domain only (SHP2^{PTP}), or SHP2 assayed with (2) partially and (3) fully activating levels of 2P-IRS-1. Compounds that inhibited only the phosphatase domain were deprioritized to enrich for potential allosteric inhibitors. Six compounds, exemplified by SHP836, demonstrated no inhibition against SHP2^{PTP}, moderate inhibitory activity (IC$_{50}$ = 5–50 μM) against SHP2 activated by 0.5 μM 2P-IRS-1, and reduced inhibitory activity in the presence of a higher concentration of 2P-IRS-1 (Fig. 2c). SHP836 was further optimized to SHP099, yielding a >70-fold improvement in biochemical potency to IC$_{50}$ = 0.071 μM (manuscript in preparation). Furthermore, SHP099 showed no detectable activity against a panel of 21 phosphatases and 66 kinases[18] (Extended Data Tables 1 and 2), and only had modest activity against 5HT3 when profiled against a preclinical safety pharmacology panel representing 49 common adverse drug reaction targets[19] (Extended Data Table 3). Importantly, SHP099 showed no activity against SHP1, the closest homologue of SHP2 sharing 61% amino acid sequence identity, supporting its high degree of target selectivity.

To understand the mechanism of inhibition, we determined the effect of the 2P-IRS-1 peptide on the potency of SHP099 and compared it to the active site inhibitor SHP043, stemming from a previously reported class of PTP1B inhibitors[20] (Fig. 2d). An increase in 2P-IRS-1 peptide correlated with a tenfold decrease in SHP099 potency, as opposed to a sixfold increase in SHP043 potency across the same range of 2P-IRS-1 peptide concentrations (Fig. 2d). These data suggest that SHP099 is interfering with the 2P-IRS-1-driven activation of SHP2, and that the active site of the PTP is more readily accessible for SHP043 binding in the activated conformation of SHP2. In addition, isothermal titration calorimetry revealed that SHP099 bound to SHP2 with 1:1 stoichiometry with a measured dissociation constant of 0.073 μM (K = 1.38 × 10^7 M^{-1}, Extended Data Fig. 3a).

To distinguish further the mechanism of inhibition from catalytic site inhibitors, we solved the crystal structure of SHP099 in complex with SHP2 (resolution, 1.7 Å) (Extended Data Table 4). Here, SHP2 was found in the same auto-inhibited, inactive conformation as the reported apo-SHP2 structure[17], with the N-terminal SH2 domain blocking the active site. Our structure revealed SHP099 bound to the central tunnel formed at the interface of the N-SH2, C-SH2, and PTP domains (Fig. 2e) and interactions between SHP099 and all three domains of SHP2, strongly suggesting that SHP099 inhibits the catalytic activity through stabilization of the inactive conformation of the enzyme. Key interactions include hydrogen bonds with Arg111 and Phe113 located on the linker between the N-SH2 and C-SH2 domains, as well as Glu250 from the PTP domain. Additionally, the dichlorophenyl group of SHP099 makes extensive hydrophobic interactions with the sidechains of Leu254, Gln257, Pro491, and Gln495 of the PTP domain (Fig. 2f). In the homologue SHP1, repositioning of the linker between the two SH2 domains would remove key SHP099 interactions (highlighted by residue Arg109 in SHP1 and Arg111 in SHP2; Extended Data Fig. 3b–d), and would yield a significantly larger central tunnel with an estimated volume of 1,012 Å^3 compared to 464 Å^3 for SHP2 and to the 262 Å^3 volume of SHP099. These observations probably explain the selectivity of SHP099 for SHP2 over SHP1.

To determine whether SHP099 was capable of cellular SHP2 inhibition, cells were treated with increasing concentrations of SHP099. SHP099 inhibited p-ERK with an IC$_{50}$ of ~0.25 μM in SHP2-dependent MDA-MB-468 and KYSE520 cells, but not in A2058 cells (Fig. 3a). No effect was observed on p-AKT levels across the same cells (Extended Data Fig. 4a). The inhibition of p-ERK was consistent with the growth inhibition observed in a colony-formation assay (Extended Data Fig. 4b). The inhibition of KYSE520, MDA-MB-468 and A2058 cells by SHP099 was also assessed in a cell proliferation assay and extended to three additional SHP2-dependent haematopoietic cell lines, MV-411, MOLM-13 and Kasumi-1, resulting in the
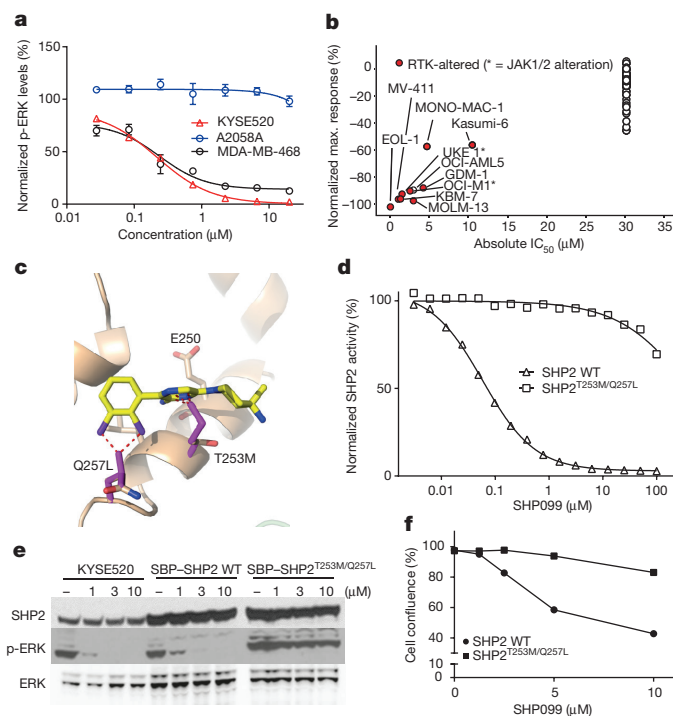

Figure 3 | Validation of SHP2-dependent inhibitory activity of SHP009 in cells. a, Inhibition of p-ERK activity by SHP099 in A2058, KYSE520 or MDA-MB-468 cells assayed by SureFire p-ERK assay. p-ERK activity is expressed as a percentage of the DMSO control. Data presented as mean ± s.d. (n = 3). **b**, Activity of SHP099 in 71 haematopoietic cell lines. The data are plotted as normalized inhibition at 30 μM SHP099 (y axis) against calculated absolute IC$_{50}$ values of SHP099 for each cell lines (x axis). Solid red circles represent cancer cells with RTK, JAK1 or JAK2 mutations, black circles correspond to NRAS- or KRAS-mutated cells. The corresponding data and cell line genotypes are in Supplementary Information Table 1. **c**, Model of engineered SHP2$^{T253M/Q257L}$ mutant highlighting steric clashes between the mutated residues and SHP099. **d**, Biochemical inhibition of wild-type SHP2 and SHP2$^{T253M/Q257L}$ by SHP099. **e**, Western blot of SHP2, p-ERK and ERK from SHP2-depleted KYSE520 cells stably re-expressing SBP-tagged wild-type SHP2 or SBP–SHP2$^{T253M/Q257L}$ and treated with SHP099 (1, 3, 10 μM). **f**, Proliferation of SHP2-depleted KYSE520 cells stably re-expressing wild-type streptavidin-binding peptide tagged (SBP) SHP2 or SBP–SHP2$^{T253M/Q257L}$ treated with SHP099 (1.25, 2.5, 5, 10 μM). Data points along the line in **d** and **f** represent the mean of two replicate values.

expected cell growth inhibition (Extended Data Fig. 4c). We further profiled SHP099 in a panel of 71 haematopoietic cancer cell lines and 26 colorectal cancer cell lines. Haematopoietic cancer cells with known alterations in oncogenic RTKs or other tyrosine kinases such as JAK1 or JAK2 were sensitive to SHP099 inhibition (Fig. 3b, Supplementary Information Table 1). Similarly, colorectal cancer cells that were sensitive to the potent Her1/2 and EGFR inhibitor Lapatinib, and hence dependent on EGFR signalling, also responded to SHP099 treatment (Extended Data Fig. 4d, Supplementary Information Table 2). In contrast, RAS- or BRAF-mutated cells from both lineages were generally resistant to SHP099 treatment (IC$_{50}$ > 30 μM for haematopoietic lines and >20 μM for colorectal lines) (Fig. 3b, Extended Data Fig. 4d and Supplementary Table 2). The observed correlation between RTK dependence and SHP099 sensitivity is robustly supported by a Chi-squared test of independence (P < 1.1 × 10^{-15}). These data therefore recapitulate the differential growth inhibitory effects observed in the shRNA screen and suggest a strong association between RTK dependence and sensitivity to SHP2 inhibition.

To determine whether SHP099-mediated suppression of MAPK signalling and growth inhibition was an on-target consequence of
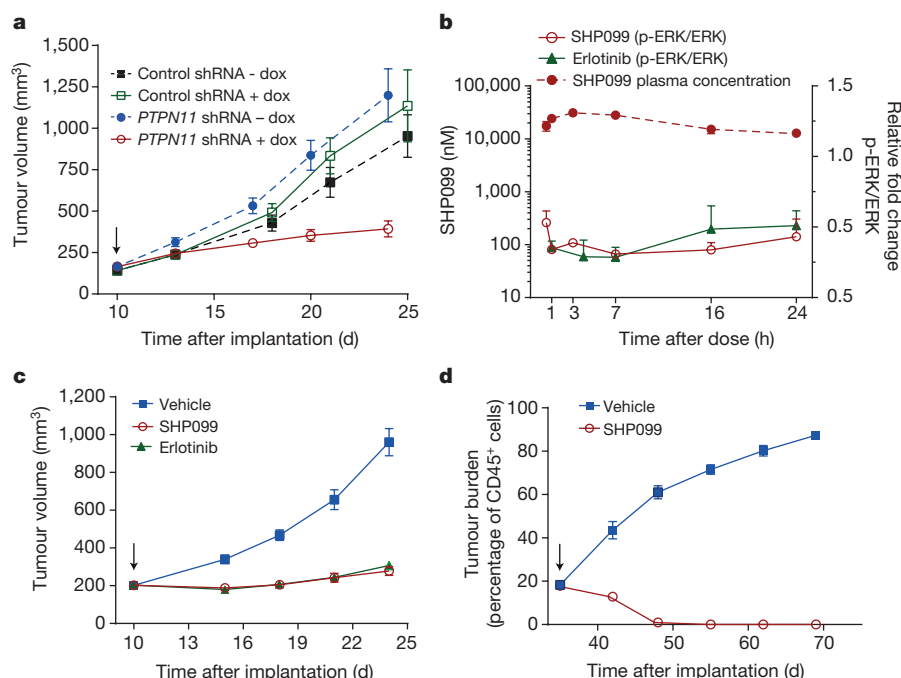
Figure 4 | *In vitro* and *in vivo* characterization of SHP099. a, SHP2 knockdown inhibits the growth of established KYSE520 xenograft tumours *in vivo*. KYSE520 cells stably expressing dox-inducible non-targeting control or *PTPN11* shRNA were inoculated into mice. Mice were treated with vehicle (dotted lines) or dox-supplemented diet (solid lines) starting 10 days after implantation. The tumour volume of vehicle or dox-treated mice is plotted as the mean ± s.e.m. (*n* = 9). **b,** *In vivo* plasma SHP099 concentration and xenograft p-ERK levels following a single oral administration of SHP099 (100 mg per kg) or erlotinib (80 mg per kg) to nude mice with subcutaneous KYSE520 xenografts. SHP099 plasma concentrations and xenograft p-ERK level were assessed through the first 24 h following compound administration.

Data are plotted as the mean ± s.e.m. (*n* = 3). **c,** Antitumour efficacy of SHP099 (100 mg per kg daily) or erlotinib (80 mg per kg daily) in nude mice bearing established subcutaneous KYSE520 xenografts. Mice were administered compounds daily by oral gavage starting 10 days after cell implantation. Data are plotted as the group mean ± s.e.m. (*n* = 9). **d,** Antitumour efficacy SHP099 (75 mg per kg) in immunocompromised mice with an orthotopic, primary-tumour-derived AML xenograft. Mice were administered SHP099 daily by oral gavage starting 35 days after tumour implantation and continued for 34 days. Tumour burden was assessed by FACS detection of hCD45^{+} leukaemic cells in circulation. Data are plotted as the group mean ± s.e.m. (*n* = 7). The arrow in **a**, **c** and **d** denotes the start of SHP099 treatment.

pharmacological inhibition of SHP2, inhibitor-resistant alleles were developed. From the co-crystal structure, we hypothesized that mutation of Thr253 and Gln257 would disrupt SHP099 binding, but maintain the integrity of the three-domain regulatory interface (Fig. 3c). After testing single- and double-mutant alleles, SHP2[T253M/Q257L] was found to retain the catalytic activity and auto-inhibited basal state of SHP2, but was 1,000-fold less sensitive to SHP099 inhibition as compared to wild-type SHP2 *in vitro* (Fig. 3d, Extended Data Fig. 3d). Treatment of KYSE520 cells expressing SHP2[T253M/Q257L] with SHP099 failed to inhibit both the signalling to p-ERK and cellular growth compared to the KYSE520 wild-type SHP2 control (Fig. 3e, f). These data strongly suggest that SHP099 inhibits MAPK signalling and proliferation in RTK-dependent cells through direct on-target inhibition of SHP2.

We next established a subcutaneous xenograft model using KYSE520 stably transduced with dox-inducible *PTPN11* shRNA to investigate whether SHP2 was required for tumour maintenance *in vivo*. Expression of *PTPN11* shRNA was induced by dox when the tumour volume reached ~200 mm[3]. SHP2 knockdown led to a significant reduction in p-ERK levels and marked tumour growth inhibition (*P* < 0.05), whereas a control non-targeting shRNA showed no effect (Fig. 4a and Extended Data Fig. 5a, b).

On the basis of its potent effects in cell culture, we next evaluated the efficacy of SHP099 in nude mice with established, subcutaneous KYSE520 xenografts. Following a single 100 mg per kg (body weight) oral dose, SHP099 yielded free plasma concentrations >10 μM and was associated with a robust inhibition of p-ERK (>50%) that was maintained for 24 h after the dose was administered (Fig. 4b). At this exposure, SHP099 was predicted to achieve a significant anti-proliferative effect on the basis of *in vitro* characterization (Fig. 3a, b and Extended

Data Fig. 4a, b). SHP099 was administered by oral gavage at 100 mg per kg daily to nude mice with KYSE520 xenografts and yielded marked tumour growth inhibition (Fig. 4c) over a 24-day time period. In a follow-up study, orally administered SHP099 showed dose-dependent anti-tumour activity in the KYSE520 xenograft model and was well tolerated, as demonstrated by insignificant or no body weight loss over the entire course of treatment (Extended Data Fig. 5c, d). For comparison, we treated a parallel cohort of KYSE520 tumour-bearing mice with the EGFR inhibitor erlotinib. The p-ERK modulation and tumour growth inhibition observed with erlotinib was equivalent to that observed with SHP099 (Fig. 4b, c). To extend this observation to the setting of RTK activation in haematological malignancies, SHP099 was evaluated in an orthotopic human-primary-tumour-derived FLT3-ITD acute myeloid leukaemia (AML) model. Here, daily dosing at 75 mg per kg led to near-complete eradication of circulating human (h)CD45^{+} leukaemic cells (Fig. 4d) and significantly reduced splenomegaly in the mice (Extended Data Fig. 5e, f). In summary, pharmacological inhibition of SHP2 by SHP099 is efficacious and well tolerated and therefore offers a novel therapeutic approach to target RTK-dependent cancers.

Despite two decades of research describing the central role of SHP2 in developmental and oncogenic signalling pathways, no SHP2 inhibitor has progressed to clinical use. Although catalytic SHP2 inhibitors have been described[11–15], they are typically of low potency and inhibit other phosphatases. Although the allosteric inhibition of a metal-dependent serine/threonine phosphatase family has been explored[21], SHP099 is the first example of a potent, selective and orally bioavailable allosteric PTP inhibitor specific to SHP2 that is efficacious and well tolerated in patient-derived tumour xenograft models. Our study provides evidence that pharmacological inhibition of SHP2 is a viable

strategy to target RTK-driven cancers and presents a new chemical tool for further interrogation of the multifaceted cellular functions of SHP2 in development, tumorigenesis, RTK-driven drug resistance and immune-checkpoint modulation.

1. Grossmann, K. S., Rosário, M., Birchmeier, C. & Birchmeier, W. The tyrosine phosphatase Shp2 in development and cancer. *Adv. Cancer Res.* **106,** 53–89 (2010).
2. Chan, R. J. & Feng, G. S. *PTPN11* is the first identified proto-oncogene that encodes a tyrosine phosphatase. *Blood* **109,** 862–867 (2007).
3. Matozaki, T., Murata, Y., Saito, Y., Okazawa, H. & Ohnishi, H. Protein tyrosine phosphatase SHP-2: a proto-oncogene product that promotes Ras activation. *Cancer Sci.* **100,** 1786–1793 (2009).
4. Mohi, M. G. & Neel, B. G. The role of Shp2 (*PTPN11*) in cancer. *Curr. Opin. Genet. Dev.* **17,** 23–30 (2007).
5. Östman, A., Hellberg, C. & Böhmer, F. D. Protein-tyrosine phosphatases and cancer. *Nat. Rev. Cancer* **6,** 307–320 (2006).
6. Gavrieli, M., Watanabe, N., Loftin, S. K., Murphy, T. L. & Murphy, K. M. Characterization of phosphotyrosine binding motifs in the cytoplasmic domain of B and T lymphocyte attenuator required for association with protein tyrosine phosphatases SHP-1 and SHP-2. *Biochem. Biophys. Res. Commun.* **312,** 1236–1243 (2003).
7. Okazaki, T., Chikuma, S., Iwai, Y., Fagarasan, S. & Honjo, T. A rheostat for immune responses: the unique properties of PD-1 and their advantages for clinical application. *Nat. Immunol.* **14,** 1212–1218 (2013).
8. Prahallad, A. *et al.* PTPN11 is a central node in intrinsic and acquired resistance to targeted cancer drugs. *Cell Reports* **12,** 1978–1985 (2015).
9. Schneeberger, V. E. *et al.* Inhibition of Shp2 suppresses mutant EGFR-induced lung tumors in transgenic mouse model of lung adenocarcinoma. *Oncotarget* **6,** 6191–6202 (2015).
10. Barretina, J. *et al.* The Cancer Cell Line Encyclopedia enables predictive modelling of anticancer drug sensitivity. *Nature* **483,** 603–607 (2012).
11. Scott, L. M. *et al.* Shp2 protein tyrosine phosphatase inhibitor activity of estramustine phosphate and its triterpenoid analogs. *Bioorg. Med. Chem. Lett.* **21,** 730–733 (2011).
12. Grosskopf, S. *et al.* Selective inhibitors of the protein tyrosine phosphatase SHP2 block cellular motility and growth of cancer cells *in vitro* and *in vivo. ChemMedChem* **10,** 815–826 (2015).
13. He, R. *et al.* Exploring the existing drug space for novel pTyr mimetic and SHP2 inhibitors. *ACS Med. Chem. Lett.* **6,** 782–786 (2015).
14. Hellmuth, K. *et al.* Specific inhibitors of the protein tyrosine phosphatase Shp2 identified by high-throughput docking. *Proc. Natl Acad. Sci. USA* **105,** 7275–7280 (2008).
15. Zeng, L. F. *et al.* Therapeutic potential of targeting the oncogenic SHP2 phosphatase. *J. Med. Chem.* **57,** 6594–6609 (2014).
16. Pluskey, S., Wandless, T. J., Walsh, C. T. & Shoelson, S. E. Potent stimulation of SH-PTP2 phosphatase activity by simultaneous occupancy of both SH2 domains. *J. Biol. Chem.* **270,** 2897–2900 (1995).
17. Hof, P., Pluskey, S., Dhe-Paganon, S., Eck, M. J. & Shoelson, S. E. Crystal structure of the tyrosine phosphatase SHP-2. *Cell* **92,** 441–450 (1998).
18. Manley, P. W. *et al.* Extended kinase profile and properties of the protein kinase inhibitor nilotinib. *Biochim. Biophys. Acta.* **1804,** 445–453 (2010).
19. Bender, A. *et al.* Analysis of pharmacology data and the prediction of adverse drug reactions and off-target effects from chemical structure. *ChemMedChem* **2,** 861–873 (2007).
20. Szczepankiewicz, B. G. *et al.* Discovery of a potent, selective protein tyrosine phosphatase 1B inhibitor using a linked-fragment strategy. *J. Am. Chem. Soc.* **125,** 4087–4096 (2003).
21. Gilmartin, A. G. *et al.* Allosteric Wip1 phosphatase inhibition through flap-subdomain interaction. *Nat. Chem. Biol.* **10,** 181–187 (2014).

METHODS

Data reporting. No statistical methods were used to predetermine sample size. The experiments were not randomized and the investigators were not blinded to allocation during outcome assessment.

Bioinformatics. Statistical analyses were performed as follows: cell counts from the pooled shRNA experiments were normalized using a quantile normalization procedure as described elsewhere[22] and normalized scores for shRNA targeting the same gene were aggregated at the gene level using the ATARIS algorithm[23]. ATARIS scores for genes of interest were binned into three categories, 'dependent', 'independent' and 'unclear' on the basis of the degree of dropout. Most RTKs show a strong phenotype in these shRNA assays, here cell lines with ATARIS score < -1 for any of the RTK genes (*EGFR*, *FRS2*, *cMET*, *ERBB2*, *FLT3*) were considered RTK-dependent, cell lines with ATARIS score > 0 were considered to be 'RTK-independent' and cell lines with ATARIS scores in between 0 and -1 were considered 'unclear' and removed from statistical analyses to remove weaker effects. An identical approach was used for comparing with RAS/RAF (BRAF, NRAS, and KRAS). SHP2 shows a less marked shRNA phenotype in these shRNA assays and the ATARIS score threshold for assigning SHP2-dependence was set to < -0.8.

Association analyses were done using a Fisher's exact test to assess (1) the association of SHP2-dependence with RTK-dependence and (2) the association of SHP2-dependence with RTK-alterations, and the odds ratio and *P* value were reported. The statistical analysis for the association of RTK-dependence and SHP099 sensitivity was performed as follows. In cell lines derived from haematological cancers, we defined RTK-dependence as RTK-altered/driven growth and in CRC lines as lapatanib sensitivity (IC$_{50} \leq 0.5 \mu$M). The *P* value was derived using the following relationships observed between RTK-dependence and sensitivity to SHP099 (IC$_{50} \leq 10 \mu$M) in all 97 lines: 80 lines are SHP099 insensitive (69 expected based on RTK independence and RAS/RAF mutation status), 0 lines are RTK-dependent and not SHP099 sensitive (10 expected), 4 lines are RTK-independent and SHP099 sensitive (14 expected), and 13 lines are both RTK-dependent and SHP099 sensitive (2 expected).

Cell culture, viral production and infection. Human cancer cell lines originated from the CCLE, authenticated by single-nucleotide polymorphism analysis and tested for mycoplasma infection[10]. Sum52, KYSE520, MDA-MB-468, KATO III, NCI-H2170, NCI-H2170, NCI-H2228, MDA-MB-231 and A2058 were cultured in RPMI medium (Invitrogen) supplemented with 10% fetal bovine serum (Invitrogen). H293 cells were grown in DMEM medium (Invitrogen) supplemented with 10% fetal bovine serum. For viral production, vectors pshSHP2 or pshNTC (nontargeting control) were transfected in H293 cells using TransIT-293 transfection reagent (Mirus Inc.), following the manufacturers protocol. At 72 h after transfection, the cell culture medium was filtered through a 0.45 μm filter, and the viral supernatant supplemented with 8 μg ml^{-1} of polybrene was used for the infection of cells. For viral infection, ~70% confluent cells in six-well dishes were infected with virus at a multiplicity of infection of 5 units per cell for 4 h and allowed to recover for 24 h with fresh medium. Stable clones were selected using either puromycin or G418. Methods for profiling small molecule inhibitors in the haematopoietic cells are described elsewhere[10]. Cells were treated using SHP099 concentration varying from 0 to 30 μM. Cellular viability was measured using CellTiter-Glo.

SHP2 allosteric inhibition assay. SHP2 is allosterically activated through binding of bistyrosylphorphorylated peptides to its Src Homology 2 (SH2) domains. The latter activation step leads to the release of the auto-inhibitory interface of SHP2, which in turn renders the SHP2 protein tyrosine phosphatase (PTP) active and available for substrate recognition and reaction catalysis. The catalytic activity of SHP2 was monitored using the surrogate substrate DiFMUP in a prompt fluorescence assay format. More specifically, the phosphatase reactions were performed at room temperature in 384-well black polystyrene plate, flat bottom, low flange, non-binding surface (Corning) using a final reaction volume of 25 μl and the following assay buffer conditions: 60 mM HEPES, pH 7.2, 75 mM NaCl, 75 mM KCl, 1 mM EDTA, 0.05% P-20, 5 mM DTT. 0.5 nM of SHP2 was co-incubated with of 0.5 μM of bisphosphorylated IRS1 peptide (sequence: H2N-LN(pY)IDLDLV(dPEG8)LST(pY)ASINFQK-amide) and 0.003–100 μM of the inhibitory compounds. After 30–60 min incubation at 25 °C, the surrogate substrate DiFMUP (Invitrogen) was added to the reaction and incubated at 25 °C for 30 min. The reaction was then quenched by the addition of 5 μl of a 160 μM solution of bpV(Phen) (Enzo Life Sciences). The fluorescence signal was monitored using a microplate reader (Envision, Perkin-Elmer) using excitation and emission wavelengths of 340 nm and 450 nm, respectively. The inhibitor dose–response curves were analysed using normalized IC$_{50}$ regression curve fitting with control-based normalization.

Protein expression and purification. Two constructs of human SHP2 (accession number NP_002825.3) were generated by cloning the *PTPN11* gene encoding truncations Met1–Leu525 (named SHP2) and Ala237–Ile529 (named SHP^{PTP}) into a pET30 vector. A coding sequence for a 6× histidine tag followed by a tomato etch virus (TEV) protease consensus sequence was added 5′ to the constructs sequence. The construct was transformed into BL21 Star (DE3) cells and grown at 37 °C in Terrific Broth containing 100 μg ml^{-1} kanamycin. At an OD$_{600}$ of 4.0, SHP2 expression was induced using 1 mM IPTG. Cells were collected after overnight growth at 18 °C.

Cell pellets were resuspended in lysis buffer containing 50 mM Tris-HCl (pH 8.5), 25 mM imidazole, 500 mM NaCl, 2.5 mM MgCl$_2$, 1 mM TCEP, 1 μg ml^{-1} DNase1, and complete EDTA-free protease inhibitor and lysed using a microfluidizer, followed by ultracentrifugation. The supernatant was loaded onto a HisTrap HP chelating column in 50 mM Tris-HCl, 25 mM imidazole, 500 mM NaCl, 1 mM TCEP and protein was eluted with the addition of 250 mM imidazole. The N-terminal histidine tag was removed with an overnight incubation using TEV protease at 4 °C. The protein was subsequently diluted to 50 mM NaCl with 20 mM Tris-HCl (pH 8.5), 1 mM TCEP then applied to a HiTrap Q FastFlow column equilibrated with 20 mM Tris (pH 8.5), 50 mM NaCl, 1 mM TCEP. The protein was eluted with a 10-column volume gradient from 50–500 mM NaCl. Fractions containing SHP2 were pooled and concentrated then loaded onto a HiLoad Superdex200 PG 16/100 column, exchanging the protein into the crystallization buffer, 20 mM Tris-HCl (pH 8.5), 150 mM NaCl and 3 mM TCEP. The protein was concentrated to 15 mg ml^{-1} for use in crystallization. QuickChange mutagenesis (Agilent) was used to generate the SHP2$^{T253M/Q257L}$ mutant using the above construct, and same procedure for expression and purification.

Chemistry. All solvents employed were commercially available 'anhydrous' grade, and reagents were used as received unless otherwise noted. A Biotage Initiator Sixty system was used for microwave heating. Flash column chromatography was performed on either an Analogix Intelliflash 280 columns (Si 50 columns (32–63 μm, 230–400 mesh, 60 Å) or on a Biotage SP1 system (32–63 μm particle size, KP-Sil, 60 Å pore size). Preparative high pressure liquid chromatography (HPLC) was performed using a Waters 2525 pump with 2487 dual wavelength detector and 2767 sample manager. Columns were Waters C18 OBD 5 μm, either 50 × 100 mm Xbridge or 30 × 100 mm Sunfire. NMR spectra were recorded on a Bruker AV400 (Avance 400 MHz) or AV600 (Avance 600 MHz) instruments. Analytical LC-MS was conducted using an Agilent 1100 series with UV detection at 214 nm and 254 nm, and an electrospray mode (ESI) coupled with a Waters ZQ single quad mass detector. One of two methods was used: (1) 3 μl of sample was injected on an inertisil C8 3 cm × 5 mm × 3 μm and eluted using a 5:95 to 95:5 acetonitrile:H$_2$O (5 mM ammonium formate) 2 min gradient; (2) 3 μl of sample was injected on an inertisil C8 3 cm × 5 mm × 3 μm and eluted using a 20:80 to5:95 acetonitrile:H$_2$O (10 mM ammonium formate) 2 min gradient. The purity of all tested compounds was determined by LC/ESI-MS data recorded using an Agilent 6220 mass spectrometer with electrospray ionization source and Agilent 1200 liquid chromatography. The mass accuracy of the system has been found to be <5 ppm. HPLC separation was performed at 75 ml min^{-1} flow rate with the indicated gradient within 3.5 min with an initial hold of 10 s. 10 mM ammonia hydroxide or 0.1 M TFA was used as the modifier additive in the aqueous phase. All compounds were found to be >95% purity.

SHP836 originated from a purchased chemical library included in the general Novartis screening chemical library. SHP836 is also known as GW286103 (ref. 24). SHP043 was synthesized as previously described[25].

6-(4-amino-4-methylpiperidin-1-yl)-3-(2,3-dichlorophenyl)pyrazin-2-amine (SHP099). A mixture of 3-bromo-6-chloropyrazine-2-amine (1.5 g, 7.2 mmol), (2,3-dichlorophenyl)boronic acid (1.37 g, 7.2 mmol), PdCl2(dppf).DCM adduct (294 mg, 0.36 mmol), and potassium phosphate (4.58 g, 21.59 mmol) in MeCN:H$_2$O (9:1, 15 ml) was stirred for 4 h at 120 °C. After cooling to room temperature, the reaction mixture was filtered through a pad of Celite followed by EtOAc wash. The solvent was removed under reduced pressure and the resulting residue was purified by silica chromatography (5 to 30% gradient of EtOAc in heptane) to give 6-chloro-3-(2,3-dichlorophenyl)pyrazin-2-amine (1.46 g, 5.32 mmol) as yellow solid. ^{1}H NMR (400 MHz, chloroform-*d*) δ ppm 7.99–8.08 (m, 1H), 7.62 (dd, *J* = 7.78, 1.76 Hz, 1 H), 7.36–7.42 (m, 1H), 7.32–7.36 (m, 1H), 4.69 (br s, 2H). ^{13}C NMR (101 MHz, chloroform-*d*) δ ppm 151.58, 146.66, 136.56, 136.30, 134.24, 132.13, 131.78, 131.56, 129.34, 128.32. HRMS calculated for C$_{10}$H$_7$Cl$_3$N$_3$ (M+H)$^+$ 273.9706, found 273.9706.

A mixture of 6-chloro-3-(2,3-dichlorophenyl)pyrazin-2-amine (125 mg, 0.455 mmol), *tert*-butyl (4-methylpiperidin-4-yl)carbamate (195 mg, 0.911 mmol), and potassium phosphate (97 mg, 0.455 mmol) in NMP (1 ml) was stirred for 36 h at 140 °C. After cooling to room temperature, the mixture was poured into a separation funnel containing saturated aqueous NH$_4$Cl and it was extracted with EtOAc (3 × 5 ml). The combined organic phases were dried over MgSO$_4$, filtered and the solvents were removed under reduced pressure. The

resulting residue was by silica chromatography (5 to 30% gradient of EtOAc in heptane) to give *tert*-butyl (1-(6-amino-5-(2,3-dichlorophenyl)pyrazin-2-yl)-4-methylpiperidin-4-yl)carbamate (113 mg, 0.250 mmol) as yellow solid. ^{1}H NMR (400 MHz, chloroform-*d*) δ ppm 7.54 (s, 1H), 7.43 (dd, *J* = 7.78, 2.01 Hz, 1H), 7.16–7.29 (m, 2H), 4.36 (br s, 1H), 4.17 (s, 2H), 3.80 (dt, *J* = 13.68, 4.33 Hz, 2H), 3.18–3.31 (m, 2H), 2.03 (br d, *J* = 13.30 Hz, 2H), 1.59 (ddd, *J* = 13.87, 10.23, 4.27 Hz, 2H), 1.35–1.42 (m, 9H), 1.32–1.35 (m, 3H). ^{13}C NMR (101 MHz, chloroform-*d*) δ ppm 154.47, 153.58, 149.85, 138.65, 133.72, 132.40, 130.33, 130.11, 127.89, 125.61, 119.19, 79.23, 50.57, 40.60 (×2), 35.83 (×2), 28.46 (×3), 28.21. HRMS calculated for $C_{21}H_{28}Cl_2N_5O_2$ (M+H)$^+$ 454.1591, found 454.1591.

A solution of *tert*-butyl (1-(6-amino-5-(2,3-dichlorophenyl)pyrazin-2-yl)-4-methylpiperidin-4-yl)carbamate (113 mg, 0.250 mmol) in THF:H$_2$O (4:1, 2.5 ml) was treated with HCl (4 M in dioxane, 230 μl, 0.928 mmol). The resulting mixture was stirred for 2 h at 140 °C. After cooling to room temperature, the volatiles were removed under reduced pressure, and the resulting residue was diluted with EtOAc (10 ml), H$_2$O (10 ml). The phases were separated and the aqueous was further extracted with EtOAc (2 × 5 ml). The combined organic phases were discarded; the aqueous phase was basified to pH 9 with NaOH 2 M, and extracted with EtOAc (3 × 10 mL). The combined organic phases were dried over MgSO$_4$, filtered and the solvent was removed under reduced pressure to afford 6-(4-amino-4-methylpiperidin-1-yl)-3-(2,3-dichlorophenyl)pyrazin-2-amine (84 mg, 0.238 mmol) as a yellow solid. ^{1}H NMR (400 MHz, methanol-*d*$_4$) δ ppm 7.61 (dd, *J* = 7.91, 1.63 Hz, 1H) 7.47 (s, 1H) 7.40 (t, *J* = 7.78 Hz, 1H) 7.34 (dd, *J* = 7.65, 1.63 Hz, 1H) 3.78 (ddd, *J* = 13.43, 7.15, 4.27 Hz, 2H) 3.50–3.64 (m, 2H) 1.55–1.75 (m, 4H) 1.25 (s, 3 H). ^{13}C NMR (101 MHz, methanol-*d*$_4$) δ ppm 155.42, 152.89, 139.87, 134.55, 133.90, 131.60, 131.48, 129.24, 125.78, 117.54, 54.84, 42.18 (×2), 39.40 (×2), 27.55. HRMS calculated for $C_{16}H_{20}Cl_2N$ (M+H)$^+$ 352.1086, found 352.1099.

Crystallization and structure determination. Sitting drop vapour diffusion method was used for crystallization, with the crystallization well containing 17% PEG 3350 and 200 mM ammonium phosphate and a drop with a 1:1 volume of SHP2 protein and crystallization solution. Crystals were formed within five days, and subsequently soaked in the crystallization solution with 2.5 mM SHP099. This was followed by cryoprotection using the crystallization solution with the addition of 20% glycerol and 1 mM of compound 1, followed by flash freezing directly into liquid nitrogen.

Diffraction data for the SHP2–SHP099 complex were collected on a Dectris Pilatus 6M Detector at beamline 17ID (IMCA-CAT) at the Advanced Photon Source at Argonne National Laboratories. The data were measured from a single crystal maintained at 100 K at a wavelength of 1 Å, and the reflections were indexed, integrated, and scaled using XDS[26]. The space group of the complex was $P2_1$ with two molecules in the asymmetric unit. The structure was determined with Fourier methods, using the SHP2 apo structure[17] (PDB accession 2SHP) with all waters removed. Structure determination was achieved through iterative rounds of positional refinement and model building using BUSTER[27] and COOT[28], yielding the published SHP2–SHP099 binary complex structure (PDB accession number 5EHR). Individual B-factors were refined using an overall anisotropic B-factor refinement along with bulk solvent correction. The solvent, phosphate ions, and inhibitor were built into the density in later rounds of the refinement. Data collection and refinement statistics are shown in Extended Data Table 4.

Isothermal titration calorimetry. The binding of SHP099 was studied by isothermal titration calorimetry (ITC) using the Auto iTC-200 calorimeter from Malvern Instruments. SHP2 was dialysed and SHP099 was dissolved into the identical buffer composed of 25 mM Hepes (pH 7.5), 100 mM NaCl, and 0.25 mM TCEP with 2% DMSO. The titration was performed at 25 °C by injecting 2.5 μl aliquots of SHP099 into the calorimetric cell (∼200 μl) containing the protein at a concentration of 55 μM. The concentration of SHP099 in the syringe was 450 μM. The heat evolved upon each injection was obtained from the integral of the calorimetric signal. The individual heats were plotted against the molar ratio, and the enthalpy change (Δ*H*) and association constant ($K_a = 1/K_d$) were obtained by nonlinear regression of the data.

p-ERK cellular assay. p-ERK cellular assay was using the AlphaScreen *SureFire* Phospho-ERK 1/2 Kit (PerkinElmer): A2058, KYSE520 or MDA-MB-468 cells (30,000 cells per well) were grown in 96-well plate culture overnight and treated with SHP099 at concentrations of 20, 6.6, 2.2, 0.74, 0.24, 0.08, 0.027 μM for 2 h at 37 °C. Incubations were terminated by addition of 30 μl of lysis buffer (PerkinElmer) supplied with the SureFire phospho-extracellular signal-regulated kinase (p-ERK) assay kit (PerkinElmer). Samples were processed according to the manufacturer's directions. The fluorescence signal from pERK was measured in duplicate using a 2101 multi-label reader (PerkinElmer EnVision). The percentage of inhibition was normalized by the total ERK signal and compared with the DMSO vehicle control.
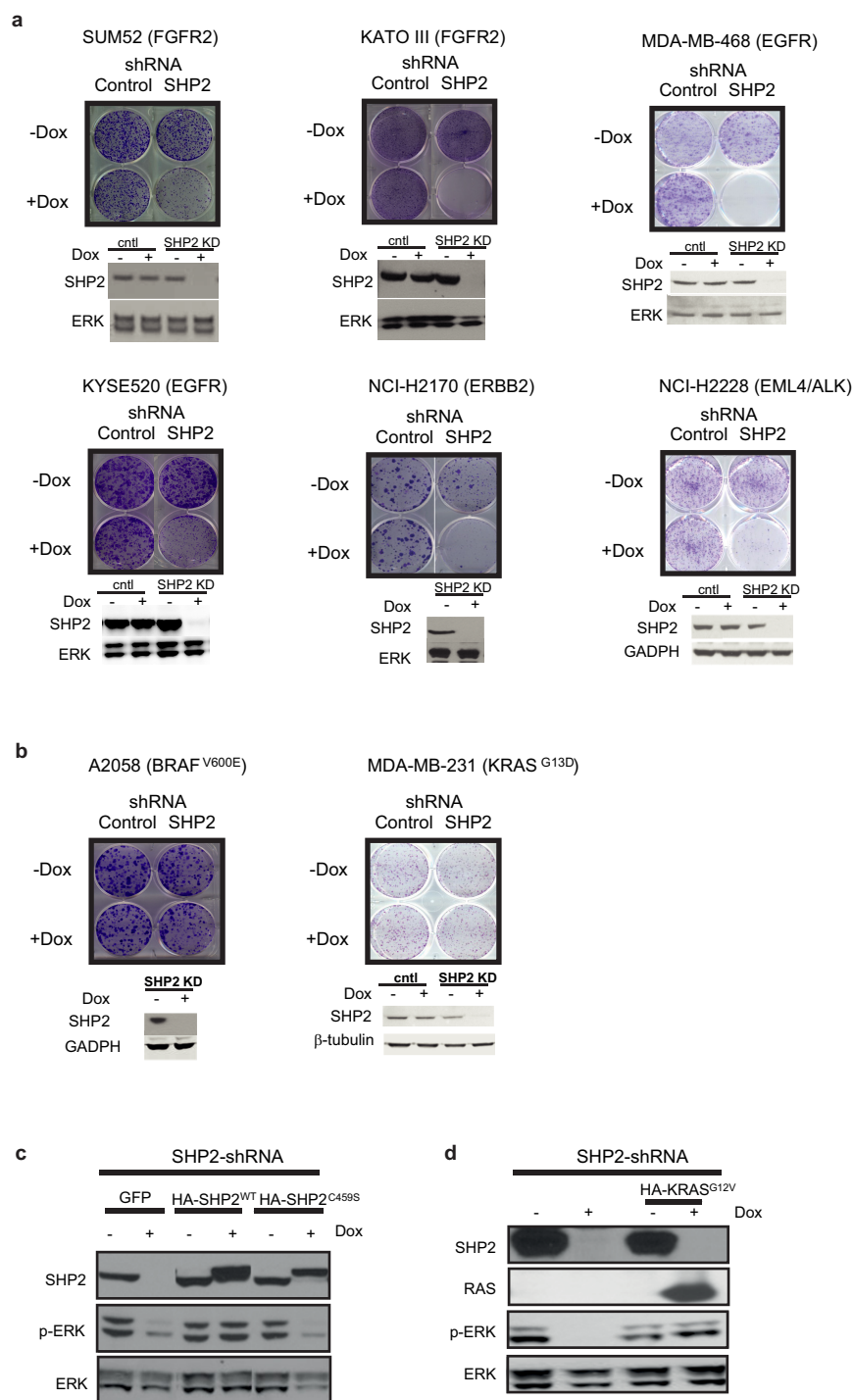
Colony formation assay and cell proliferation assay. KYSE520, MDA-MB-468, A2058, Sum52, KatoIII cells (1500 cells per well) were plated onto 24-well plates in 300 μl medium (RPMI-1640 containing 10% FBS, Lonza). For drug treatment, SHP099 were added at various concentrations (10, 5, 2.5, 1.25 μM) 24 h and 5 days after cell plating. At day 11, colonies were stained with 0.2% crystal violet (MP Biomedicals) and subsequently dissolved in 20% acetic acid for quantitation using a Spectramax reader (Thermo Scientific). In cell proliferation assay, KYSE520, A2058 and colorectal cancer cells (1500 cells per well) were plated onto 96-well plates in 100 μl medium (RPMI-1640 containing 10% FBS, Lonza) and treated with SHP099 and/or lapatinib concentration varying from 0.0 to 20.25 μM. At day 5, 50 μl CellTiter-Glo reagent (Promega) was added, and the luminescent signal was determined according to the supplier's instruction (Promega). Method of profiling SHP099 in the haematopoietic cancer cell panels were described previously[10]. Cells were treated using SHP099 concentration varying from 0.0 to 30 μM. Cellular viability was measured using CellTiter-Glo at day 3.

Western blotting. Cells were lysed on ice for 30 min with CST lysis buffer (Cell Signaling) containing phosSTOP (Roche). Cell lysates were centrifuged at 4 °C for 15 min with a microfuge. Protein concentrations of cell lysate supernatants were measured. Cell lysate supernatants of equal-amount proteins were used for immunoblotting. The following antibodies were used: SHP2 (Santa Cruz SC-280), pERK (CST #4377S), ERK (Santa Cruz SC-93), RAS (CST#3965S), pAKT (CST #4060S), GAPDH (CST #2118S).

Tumour xenograft experiments and tissue-sample preparations. All animal studies were carried out according to the Novartis Guide for the Care and Use of Laboratory Animals. Cell lines were confirmed to be devoid of mycoplasma and mouse viruses before use. Sample sizes were determined roughly on the basis of a power analysis using historical internal xenograft tumour volume data and anti-tumour responses. In the efficacy studies, animals were randomly assigned to treatment groups by an algorithm that moves animals around to achieve the best case distribution to assure that each treatment group has similar mean tumour burden and standard deviation. Female athymic nude mice (9–12 weeks of age) were inoculated subcutaneously (3 × 10^6 cells in a suspension containing 50% phenol red-free matrigel (BD Biosciences) in Hank's balanced salt solution) with parental KYSE520 cells or KYSE520 cells stably expressing dox-inducible control non-targeting shRNA or distinct *PTPN11*-targeting shRNA. For pharmacokinetic/pharmacodynamics study, mice were administered a single dose of vehicle control, erlotinib, or SHP099 by oral gavage once tumours reached roughly 500 mm^3. Mice were subsequently killed at predetermined time points following a single dose of compound, at which point plasma and xenograft fragments were collected for determination of SHP099 concentrations and p-ERK modulation, respectively. For efficacy studies, xenograft tumours were measured twice weekly by calipering in two dimensions. Once tumours reached roughly 200 mm^3, mice were randomly assigned to treatment groups. For the shRNA study, on day 10 after cell line implantation, mice were assigned to receive either vehicle diet (standard diet) or dox-supplemented diet (Mod LabDiet 5053, 400 p.p.m. dox) for the duration of the study. For the efficacy study, on day 10 after cell line implantation, mice were assigned to receive either vehicle, SHP099 (100 mg per kg daily), or erlotinib (80 mg per kg daily) by oral gavage. In both efficacy studies, tumour volume and mouse body weight was assessed twice weekly. To assess MAPK pathway modulation in xenograft protein lysates, total and phospho ERK1/2 was assessed using a commercially available kit (Meso Scale Discovery catalogue number K15107D). The assay was conducted as recommended by Meso Scale Discovery with the exception that protein lysate was incubated overnight. The development of the patient-derived AML xenograft model in mice and study design has been previously described[29]. An additional group of mice (*n* = 7) was added to the study on day 35 after tumour implantation and treated with SHP099 (75 mg per kg daily) for 34 days. At the end of the study (69 days after tumour implantation), mice were euthanized, and spleen weights of individual mice were recorded. In all cases, no data or animals were excluded and results are expressed as mean and standard error of the mean. No further statistical analysis was performed.

Pharmacokinetics. Plasma samples were precipitated and diluted with acetonitrile containing internal standard and prepared for LC-MS/MS. An aliquot (20 μl) of each sample was injected into the API4000 LC-MS/MS system for analysis, and transitions of 352.05 AMU (Q1) and 267.10 AMU (Q3) were monitored. All pharmacokinetic parameters were derived from concentration–time data by noncompartmental analyses. Pharmacokinetic parameters were calculated using the computer program WinNonlin (Version 6.4) purchased from Certara Company. Results are expressed as mean and standard error of the mean. No further statistical analysis was performed.

22. Hoffman, G. R. *et al.* Functional epigenetics approach identifies BRM/SMARCA2 as a critical synthetic lethal target in BRG1-deficient cancers. *Proc. Natl Acad. Sci. USA* **111,** 3128–3133 (2014).
23. Shao, D. D. *et al.* ATARiS: computational quantification of gene suppression phenotypes from multisample RNAi screens. *Genome Res.* **23,** 665–678 (2013).
24. Clare, J. J., Tate, S. N., Nobbs, M. & Romanos, M. A. Voltage-gated sodium channels as therapeutic targets. *Drug Discov. Today* **5,** 506–520 (2000).
25. Zhao, H. *et al.* Isoxazole carboxylic acids as protein tyrosine phosphatase 1B (PTP1B) inhibitors. *Bioorg. Med. Chem. Lett.* **14,** 5543–5546 (2004).
26. Kabsch, W. XDS. *Acta Crystallogr. D* **66,** 125–132 (2010).
27. Bricogne, G. *et al.* BUSTER version 2.8.0. (Global Phasing Ltd., 2009).
28. Emsley, P., Lohkamp, B., Scott, W. G. & Cowtan, K. Features and development of Coot. *Acta Crystallogr. D* **66,** 486–501 (2010).
29. Weisberg, E. *et al.* Inhibition of wild-type p53-expressing AML by the novel small molecule HDM2 inhibitor CGM097. *Mol. Cancer Ther.* **14,** 2249–2259 (2015).

a

SUM52 (FGFR2)

KATO III (FGFR2)

MDA-MB-468 (EGFR)

KYSE520 (EGFR)

NCI-H2170 (ERBB2)

NCI-H2228 (EML4/ALK)

b

A2058 (BRAF^{V600E})

MDA-MB-231 (KRAS^{G13D})

c

d

Extended Data Figure 1 | SHP2 depletion inhibits the growth of RTK-amplified cancer cells. a, Cells expressing dox-inducible SHP2 shRNA in various RTK-amplified cancer cells were generated including SUM52 (FGFR2), KATOIII (FGFR2), MDA-MB-468, KYSE520 (EGFR), NCI-H2190 (HER2), NCI-H2228 (EML4-ALK). **b**, Stable clones of MDA-MB-231 (KRAS^{G13D}) and A2058 BRAF^{V600E}) cancer cells were established as controls. Cells were treated with dox, and colony formation was measured after 11 days by crystal violet staining. **c**, Western blot showing the expression of SHP2, p-ERK and ERK in the presence ($+$) or absence ($-$) of dox in MDA-MB-468 SHP2-depleted cells stably expressing either GFP, wild-type HA–SHP2 or HA–SHP2^{C459S}. **d**, Western blot of SHP2, p-ERK and ERK in the presence ($+$) or absence ($-$) of dox in SHP2-depleted SUM52 cells expressing vector control or HA–KRAS^{G12V}. In **c** and **d**, dox treatment induces depletion of endogenous SHP2 protein and simultaneously expression of the exogenous proteins GFP, wild-type HA–SHP2, HA–SHP2^{C459S} or HA–KRAS^{G12V}.
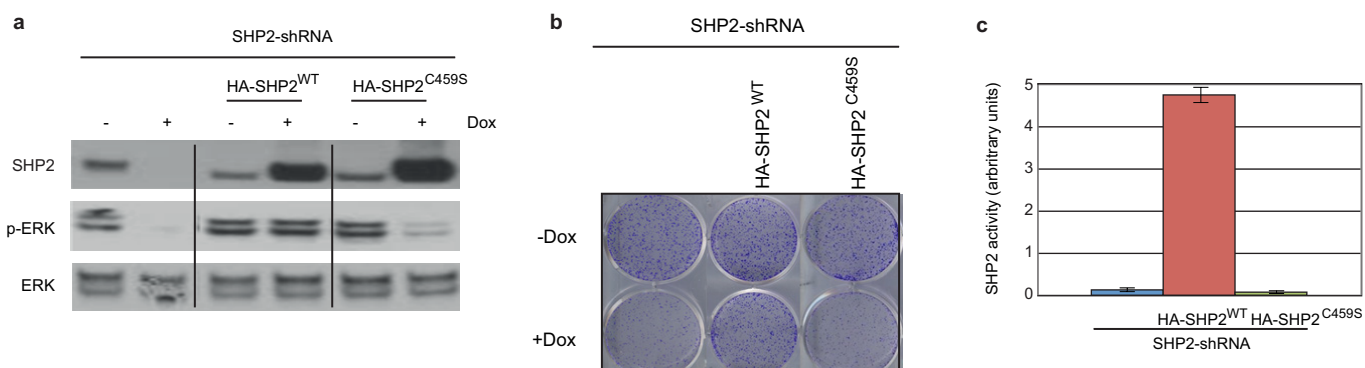
Extended Data Figure 2 | Phosphatase activity is required for cancer growth. a, Western blot of SHP2, p-ERK and ERK in SHP2-depleted SUM52 cells stably expressing vehicle, wild-type SHP2 or HA–SHP2^C459S. Note, four lanes corresponding to an unrelated study were removed from the image. All lanes originated from the same gel at the same exposure. **b**, Colony formation of SHP2-depleted SUM52 cells stably expressing vehicle, wild-type SHP2 or HA–SHP2^C459S. SHP2 knockdown and SHP2 variant re-expression per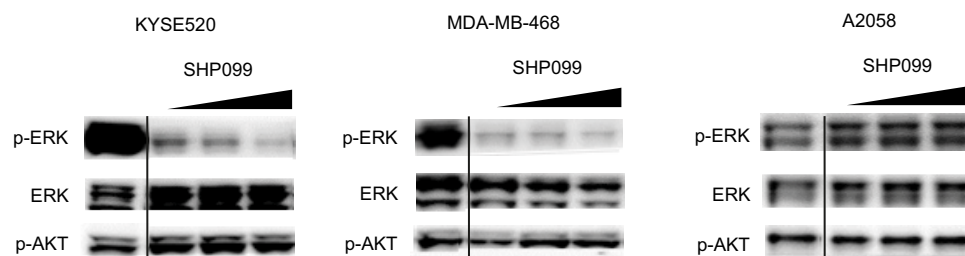form using dox treatment. Colony formation was monitored after 11 days with crystal violet staining. **c**, Phosphatase activity of SHP2-depleted SUM52 cells stably expressing HA–SHP2 or HA–SHP2^C459S. Cells were treated with dox for 3 days. SHP2 protein was immunoprecipitated from cell lysates and phosphatase activity was measured using DiFMUP assay. Data are presented as mean ± s.d. ($n = 3$).
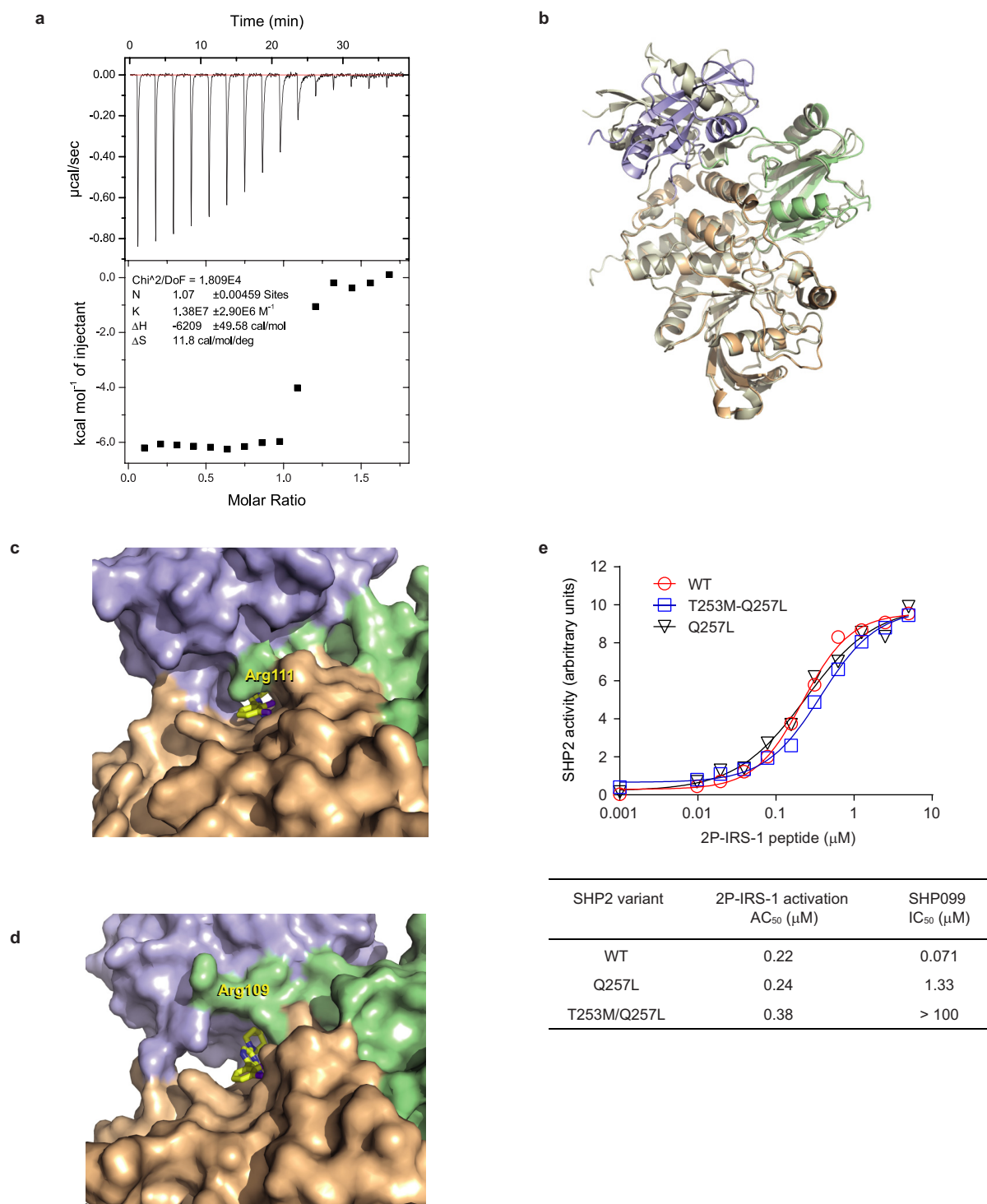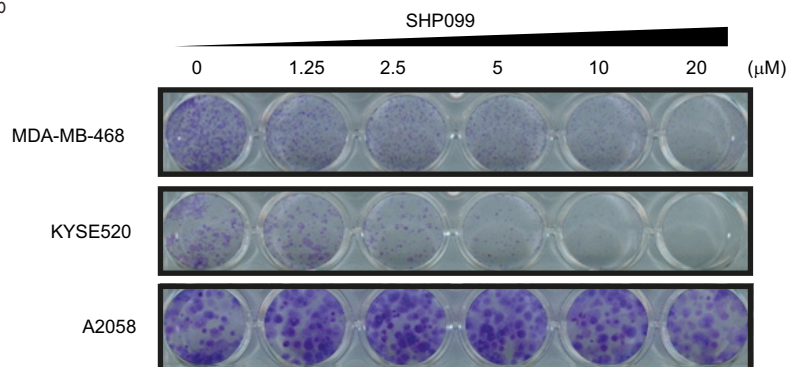
Extended Data Figure 3 | Thermodynamic characterization of the SHP099–SHP2 binding complex, comparison of SHP2 and SHP1's allosteric pocket and characterization of SHP099-resistant SHP2 mutants. a, Isothermal titration calorimetry of SHP099 binding to SHP2. SHP099 binds stoichiometrically to SHP2 with a dissociation constant measured at 73 ± 15 nM. **b**, Structural differences in the central tunnel between SHP1 and SHP2. Ribbon representation of SHP2 (multi-colour) and SHP1 (grey) X-ray structures in the closed conformation. The PTP (tan) and N-SH2 (green) domain overlay well (r.m.s.d. < 1.5 Å), however the C-SH2 (blue) domain has a significantly different orientation. **c**, Surface representation of SHP2–SHP099 co-crystal structure. **d**, Surface representation of SHP1 with SHP099 modelled on the basis of the SHP2

superimposition. Central tunnel is significantly larger in SHP1 owing to a change in orientation of the C-SH2 domain. This change repositions the linker between the two SH2 domains removing several key interactions, highlighted by residue Arg109 in SHP1 and by Arg111 in SHP2 (equivalent residues). **e**, Biochemical activity of wild-type SHP2, SHP2^{Q257L} and SHP2$^{T253M/Q257L}$. SHP2 activity was determined using DiFMUP in the presence of various concentrations of 2P-IRS-1. Data points along the line represent the mean of two replicate values. SHP2^{Q257L} and SHP2$^{T253M/Q257L}$ retain activity regulation and 2P-IRS-1 activation potential comparable to wild-type SHP2 but are 18- and <1,000-fold less sensitive to SHP099 inhibition.
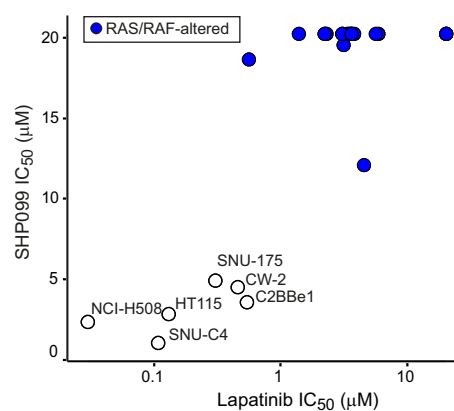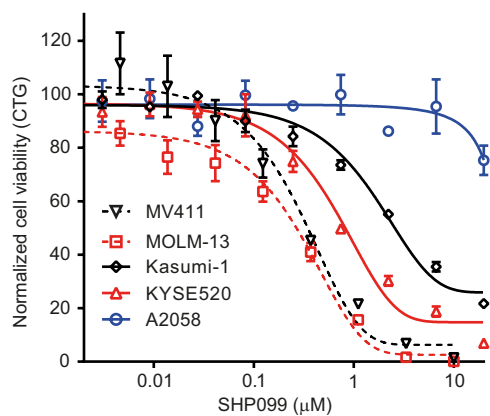
SHP2 variant	2P-IRS-1 activation AC$_{50}$ (μM)	SHP099 IC$_{50}$ (μM)
WT	0.22	0.071
Q257L	0.24	1.33
T253M/Q257L	0.38	> 100

Extended Data Figure 4 | Cellular activity of SHP099. a, Western blot of SHP2, p-ERK, ERK and p-AKT from KYSE520, MDA-MB-468 or A2058 cells treated with SHP099 (1, 3, 10 μM). Note, three lanes corresponding to an unrelated study were removed from the image. All lanes originated from the same gel at the same exposure. **b**, Colony formation of KYSE520, MDA-MB-468, and A2058 in the presence of SHP099. Colony formation was measured after 11 days of SHP099 treatment by crystal violet staining. **c**, SHP099 inhibitory activity against cell lines KYSE520 (EGFR-amplified), MV-411(FLT3-ITD), MOLM-13 (FLT3-ITD), Kasumi

(c-Kit altered) and negative control A2058 (BRAF^{V600E}) treated with SHP099 concentration varying from 0.0046 to 20 μM. Cellular viability was measured using CellTiter-Glo. Data presented as mean ± s.d. ($n = 3$). **d**, Comparison of SHP099 activity with Lapatinib in a panel of 26 colorectal cell lines. SHP099 sensitivity correlates with sensitivity to Lapatinib, a potent tyrosine kinase inhibitor against Her1/2 and EGFR. RAS- and BRAF-mutated cell lines are shown in blue. Cellular viability was measured using CellTiter-Glo. The corresponding data and cell line genotypes are included in Supplementary Information Table 2.

a

b

c

d

e

f
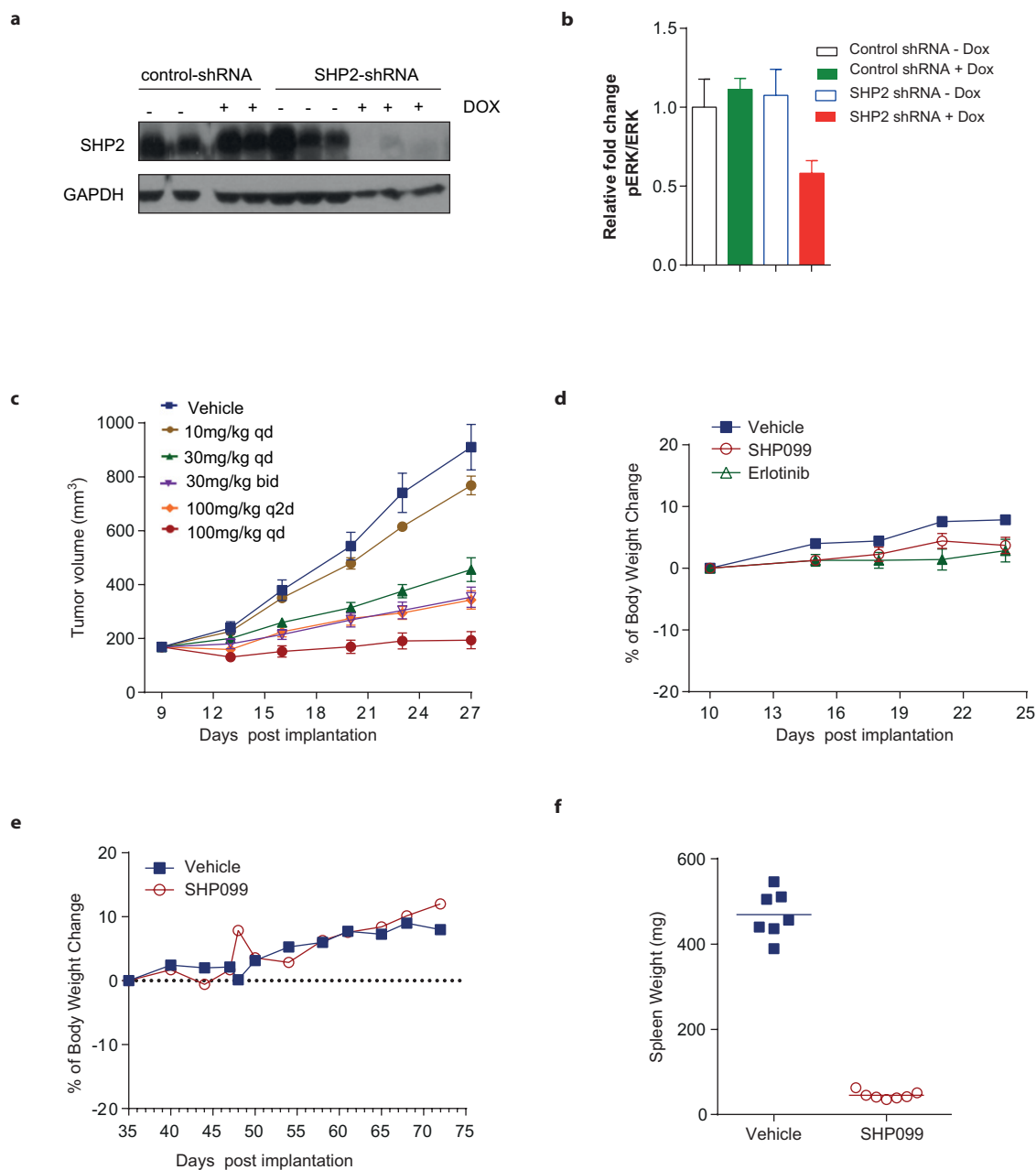
Extended Data Figure 5 | SHP2 depletion or inhibition by SHP099 assessed in *in vivo* xenograft models. a, Western blot of SHP2 and GAPDH in KYSE520 xenograft lysates following 14 days of dox treatment (+). **b**, Response of p-ERK in tumour xenograft lysates following 14 days of dox treatment. **c**, Antitumour efficacy of SHP099 administered orally for 14 consecutive days at the doses and schedules indicated. Data are plotted as the treatment mean $\pm$ s.e.m. ($n = 9$). **d**, Body weight of mice bearing subcutaneous KYSE520 xenografts and administered either SHP099 (100 mg per kg daily), erlotinib (80 mg per kg daily) or vehicle for 14 consecutive days. Data are presented as treatment mean $\pm$ s.e.m. ($n = 7$). **e**, Body weight of mice bearing orthotopic primary tumour derived xenografts and administered an oral gavage of SHP099 at 75 mg per kg daily. Data are presented as treatment mean $\pm$ s.e.m. ($n = 7$). **f**, The mouse spleen weight measurement of mice bearing the orthotopic AML xenograft model following 34 days of once-daily dosing with SHP099 at 75 mg per kg. Data are presented as treatment mean $\pm$ s.e.m. ($n = 7$).

Extended Data Table 1 | Selectivity profiling of SHP099 in phosphatase enzyme panel

Eurofins Phosphatase	Species	Native phosphatase sequence present in recombinant protein	IC$_{50}$, μM
CD45(h)	Human	598-end	>100
DUSP22(h)	Human	Full length	>100
HePTP(h)	Human	22-end	>100
LMPTP-A(h)	Human	Full length; Q106R	>100
LMPTP-B(h)	Human	Full length	>100
MKP5(h)	Human	320-end	>100
PP1a(h)	Human	Full length	>100
PP2A(h)	Human	Native enzyme	>100
PP5(h)	Human	Full length	>100
PTPb(h)	Human	1643-end	>100
PTP-1B(h)	Human	1-321	>100
PTP MEG1(h)	Human	423-end	>100
PTP MEG2(h)	Human	283-end	>100
PTPN22(h)	Human	1-312	>100
RPTPm(h)	Human	879-1184	>100
SHP-1(h)	Human	Full length	>100
SHP-2(h)	Human	230-545	>100
TCPTP(h)	Human	1-341	>100
TMDP(h)	Human	Full length	>100
VHR(h)	Human	Full length	>100
YopH(Yersinia)	Yersinia	Full length; R211A	>100

Assay was performed using PhosphataseProfiler at Eurofins.

Extended Data Table 2 | Selectivity profiling of SHP099 in kinase enzyme panel

Kinases	IC$_{50}$, μM	Kinases	IC$_{50}$, μM
CE ABL1 (64-515) nonphos v2	>10	CE MAPK1	>10
CE ACVR1 (172-499)	>10	CE MAPK10	>10
CE AKT1	>10	CE MAPK14	>10
CE ALK (1066-1459)	>10	CE MAPKAPK2	>10
CE AURKA	>10	CE MAPKAPK5 (2-472)	>10
CE BTK	>10	CE MET (956-1390)	>10
CE CAMK2D	>10	CE MKNK1	>10
CE CDK1B	>10	CE MKNK2	>10
CE CDK2A	>10	CE PAK2	>10
CE CDK4D1	>10	CE PDGFRa (551-V561D-1089)	>10
CE CSK	>10	CE PDPK1	>10
CE CSNK1G3 (35-362)	>10	CE PIM2	>10
CE EGFR (668-1210)	>10	CE PKN1	>10
CE EPHB4 (566-987)	>10	CE PKN2	>10
CE ERBB4 (673-1308)	>10	CE PLK1	>10
CE FGFR1 (407-822)	>10	CE PRKACA	>10
CE FGFR2 (406-821)	9.7	CE PRKCA	>10
CE FGFR3 (411-806)	>10	CE PRKCQ	>10
CE FGFR3 (411-K650E-806)	>10	CE RET (658-1072)	>10
CE FGFR4 (388-802)	>10	CE ROCK2 (6-553)	>10
CE FLT3 (563-D835Y-993)	>10	CE RPS6KB1 (1-421)	>10
CE GSK3B	9.9	CE SRC (1-535)	>10
CE INSR (871-1343)	>10	CE STK17B	>10
CE IRAK1 (184-712)	>10	CE SYK (2-635) nonphos	>10
CE IRAK4 (1-460)	>10	CE WNK1 (2-491)	>10
CE JAK1 (866-1154)	>10	CE ZAP70	>10
CE JAK2 (808-1132)	>10	ADP-FRET PIK3CD	>10
CE KDR (807-1356)	>10	ADP-FRET PIK3CG	>10
CE KIT (544-976)	>10	ATP-binding MTOR(1360-2549)	>10
CE LCK (1-508)	>10	KGlo PIK3C3	>10
CE LYN (1-512)	>10	KGlo PIK3CA	>10
CE MAP3K8 (30-404)	>10	KGlo PIK3CB	>10
CE MAP4K4	>10	KGlo PIK4CB	>10

Extended Data Table 3 | Preclinical safety pharmacology off-target activity panel

Assay	AC$_{50}$ (µM)	
	Antagonism	Agonism
5HT2C	>30	N/A
Ad1	>30	N/A
Ad2A	>30	N/A
Ad3	>30	N/A
alpha2B	>30	N/A
alpha2C	>30	N/A
beta1	>30	N/A
AT1	>30	N/A
CCKa	>30	N/A
D2	>30	N/A
D3	>30	N/A
ETa	>30	N/A
GHS	>30	N/A
H1	>30	N/A
H3	>30	N/A
MC3	>30	N/A
h Motilin	>30	N/A
M1	>30	N/A
M3	>30	N/A
op-delta	>30	N/A
op-mu	>30	N/A
hr V1a	>30	N/A
Nic(ns)	>30	N/A
5HT3	6.7	N/A
AdT	>30	N/A
DAT	>30	N/A
NET	>30	N/A
5HTT	>30	N/A
COX-1	>30	N/A
COX-2	14	N/A
MAO-A	>30	N/A
h PDE3	>30	N/A
5HT1A	> 30	> 30
5HT2A	> 30	> 30
5HT2B	> 30	> 30
Alpha 1A	> 30	> 30
Alpha 2A	> 30	> 30
Beta2	> 30	N/A
CB1	> 30	> 30
D1	> 30	N/A
GABAA	> 30	> 30
M2	> 30	> 30
rr AR	> 30	N/A
ERalpha	12	> 10
GR	> 30	> 30
PPARg	> 30	> 30
PR-B	> 30	> 30
PXR	> 30	> 30

Extended Data Table 4 | Crystallographic Data and Refinement Statistics

Parameters	SHP2/SHP099 complex
Space group	$P2_1$
Unit Cell (Å)	a=46.19, b=213.79, c=55.89
Resolution range (Å)	24.89 – 1.70 (1.74 – 1.70)
Total observations	371305
Unique reflections	114992
Completeness (%)[a]	97.8 (87.3)
Multiplicity	3.2 (2.4)
$<I/\sigma(I)>$[a]	17.5 (2.4)
R_{merge}[a,b]	0.034 (0.373)
R_{cryst}/R_{free}[c]	0.195/0.221 (0.235/0.257)
Protein atoms	7768
Heterogen atoms	76
Solvent molecules	670
Average B-factor (Å^2)	27.4
R.m.s.d. bond lengths (Å)	0.01
R.m.s.d. bond angle (°)	1.02
Ramachandran Plot (%)	
Favored	97.1
Allowed	2.3
Outliers	0.6

[a]Numbers in parentheses are for the highest resolution shell.
[b]$R_{merge}=\Sigma|I_h-<I_h>|/\Sigma I_h$ over all h, where I_h is the intensity of reflection h.
[c]R_{cryst} and $R_{free}=\Sigma||F_o|-|F_c||/\Sigma|F_o|$, where F_o and F_c are observed and calculated amplitudes, respectively. R_{free} was calculated using 5% of data excluded from the refinement.